JTTEE5 24:720–728
DOI: 10.1007/s11666-015-0226-2
1059-9630/$19.00 © ASM International

Peer Reviewed

Ceramic Nano-particle/Substrate Interface Bonding Formation Derived from Dynamic Mechanical Force at Room Temperature: HRTEM Examination

Hai-Long Yao, Guan-Jun Yang, Sheng-Qiang Fan, Cheng-Xin Li, and Chang-Jiu Li

(Submitted October 18, 2014; in revised form December 18, 2014)

The bonding of TiO_2 nano-particle/substrate is a critical factor influencing the performance of dye-sensitized solar cells. In order to reveal the bonding properties at TiO_2 nano-particle/substrate interface, high-resolution transmission electron microscopy (HRTEM) analysis was adopted to TiO_2 coatings prepared by three different approaches. In the HRTEM analysis, the effective bonding mode is allowed to distinguish from the false image overlapping. Results show that large areas of effective bonding between nano-TiO_2 particles and the substrate surface formed in the room temperature cold sprayed coating and mechanically pressed coating, while only limited interface areas with the effective bonding were observed in the coating deposited by non-pressed method. These results confirm that both high impact pressure during the room temperature cold spraying and mechanical pressure contribute to the bonding formation at the particle/substrate interface.

Keywords HRTEM, interface, pressure, room temperature cold spraying, titania

1. Introduction

Dye-sensitized solar cells (DSCs) are regarded as an alternative to the conventional Si-based solar cells owing to their low production cost relative to the high energy conversion efficiencies (Ref 1-4). The device structure is composed of a photoanode, a liquid or solid state electrolyte, and a counter electrode (Ref 1). The photoanode is prepared by adsorbing dye molecules on the surface of a nanoporous TiO_2 coating, which is fabricated by depositing nano-TiO_2 particles on a conductive substrate. Upon light illumination, dye molecules are excited, injecting electrons into the conduction band of the TiO_2 and then regenerated by the electrolyte. The injected electrons need to transport across TiO_2 nano-particles in the TiO_2 coating and then pass through the interface of TiO_2/substrate before they are collected by the transparent conductive layer of the substrate (Ref 1). Previous reports have shown that the electron transport at TiO_2/substrate interface is much more crowded than that within the TiO_2 film (i.e., via TiO_2 particle/particle interface) (Ref 5, 6). If an electron transport pathway is called one ''lane,'' the available lanes within the TiO_2 film are two orders of magnitude higher than those at the TiO_2/substrate interface. In this regard, the physical and electronic nature of the interface at TiO_2/substrate is much more important for the successful collection of the photo-induced electrons (Ref 1-4).

In order to improve the interface bonding for both TiO_2/substrate and TiO_2 particle/particle and hence to decrease the series electrical resistance for the DSC, the TiO_2 film is usually annealed at a high temperature, i.e., ~500 °C, before it is assembled in the DSC devices (Ref 7-9).

However, plastic substrates for assembly of flexible DSCs cannot bear a temperature higher than 150 °C (Ref 10, 11). In this case, the bonding at the particle/particle interfaces and coating/substrate interfaces needs to be enhanced by other methods, such as mechanical pressing (Ref 12-16) and dynamic pressure as in room temperature cold spraying (Ref 17-19). Investigations have shown that the DSC efficiencies can be significantly increased by increasing pressure during mechanical pressing (Ref 12-16) and increasing particle velocity and thereby impact pressure during room temperature cold spraying (Ref 17-19). An increased electron transport coefficient can be observed after high pressure pressing (Ref 14, 20), which is attributed to the improved particle/particle connection (Ref 19-26). However, the effect of pressing on the contact at the coating/substrate interface and its contribution to the DSC performance have not been investigated in full detail (Ref 19-22). Most importantly, it was found that the overall photo-to-electric energy conversion efficiency of plastic

Hai-Long Yao, Guan-Jun Yang, Cheng-Xin Li, and **Chang-Jiu Li**, State Key Laboratory for Mechanical Behavior of Materials, School of Materials Science and Engineering, Xi'an Jiaotong University, Xi'an 710049, China; and **Sheng-Qiang Fan**, School of Chemistry & Molecular Biosciences, The University of Queensland, St Lucia, QLD 4072, Australia. Contact e-mails: ygj@mail.xjtu.edu.cn and licj@mail.xjtu.edu.cn.

DSCs is still lower than that of glass-based DSCs using a high temperature sintered photoanode even though the particle/particle connection property is similar for the both types of DSCs (Ref 21, 22). Those facts clearly suggest that the physical and electronic properties of the coating/substrate interface may be critical to the DSC performance, which therefore deserves further exploration.

To understand the properties of electron transportation in the photoanode, electrochemical impedance spectroscopy (EIS) analysis has been widely used (Ref 4, 5, 23). However, the impedance owing to the coating/substrate cannot be extracted as it is mixed with the impedance for the counter electrode (Ref 5, 23, 24). Therefore, several indirect methods are employed to investigate the coating/substrate interface bonding. For example, the mechanical property of the coating/substrate interface was explored by an ultrasonic cleaning method (Ref 25-28). Although this approach can qualitatively indicate the coating/substrate interface adhesion, it is a macroscopic method without the details for the coating/substrate microstructure. Similarly, a nano-scratch technique was applied to detect the microscopic stress of the coating/substrate interface (Ref 25, 26). However, it turns out that the stress comes from not only the coating/substrate interface but also the coating itself due to its high porosity. Therefore, these mechanical approaches are still not effective ways to reflect the properties of the coating/substrate contact, especially the detailed microstructure of the coating/substrate contact.

To explore the structure/property relationship of the coating/substrate interface, it is essentially important to characterize the microstructure of coating/substrate interface directly by microscopy technologies. Transmission electron microscopy (TEM) has been applied to examine the coating/substrate microstructure for the nanoporous TiO_2 coating in DSCs (Ref 29). From the TEM images, it is clear that the nanoporous TiO_2 coating completely adhered to the substrate. However, the detailed microstructure of the individual particle/substrate contact was not revealed (Ref 29). Since the porous coating is composed of nano-sized TiO_2 particles, the properties of coating/substrate contact should be mainly determined by the individual particle/substrate contacts (Ref 5, 7). Due to the small size (generally from 10 to 25 nm) of the nanoparticles, it remains a challenge to examine the detailed microstructure of TiO_2 coating/substrate interface.

In this study, the detailed microstructure of the interface between TiO_2 coating and the substrate was investigated by high-resolution transmission electron microscopy (HRTEM). The TiO_2 coatings fabricated by room temperature cold spray were employed for the investigation, and the screen-printed and mechanical-pressed coatings were also used for comparison.

2. Experimental Procedure

2.1 Screen-Printed TiO_2 Coating

A binder-free paste consisting of TiO_2 nano-powder (P25, Degussa, Dusseldorf, Germany) of 25 nm in diameter and ethanol was prepared according to literature (Ref 15, 16). It was then applied onto a substrate surface by a screen printing (Ref 15, 16). In order to facilitate the preparation of very thin coating for the observation through HRTEM, F-doped SnO_2-glass substrate (FTO, TEC-15, LOF, Ohio, USA) was used instead of a plastic-based substrate. The coating was dried under ambient condition.

2.2 Mechanical-Pressed TiO_2 Coating

After evaporation of the ethanol, the as-received screen-printed TiO_2 coating was put between two planar steel press plates, and a pressure of 150 MPa (Ref 12-16) was applied using a hydraulic press (769YP-24B, Longtuo, Shanghai, China).

2.3 Room Temperature Cold Sprayed TiO_2 Coating

TiO_2 coating was deposited using a lab-developed room temperature cold spray system (Ref 17-19). During the cold spraying, TiO_2 nano-particles are accelerated to high velocity and impact on conductive FTO substrate surface to form a porous TiO_2 coating. Helium was used as the accelerating gas at a flow rate of 7.5 L/min. The chamber pressure during spraying was lower than 1000 Pa. The standoff distance from the nozzle exit to the conductive FTO substrate surface was 15 mm. The relative traverse speed of the nozzle over the substrate was 20 mm/s.

2.4 Characterization of TiO_2 Coating Microstructure

The crystalline structure of both the coatings and feedstock powder was characterized by x-ray diffraction (XRD) analysis (Shimadzu XRD-6000, Kyoto, Japan) with Cu Kα radiation ($\lambda = 0.15418$ nm). Surface morphologies of the coatings were examined by scanning electron microscopy (SEM) (Quanta 200, FEI, Eindhoven, Netherlands). The microstructure of coating/substrate interface in the TiO_2 coatings was characterized by TEM (JEM-2100F, JEOL, Tokyo, Japan). The cross-sectional coating samples for TEM examination were prepared by gluing the coating in the face-to-face configuration, pol-

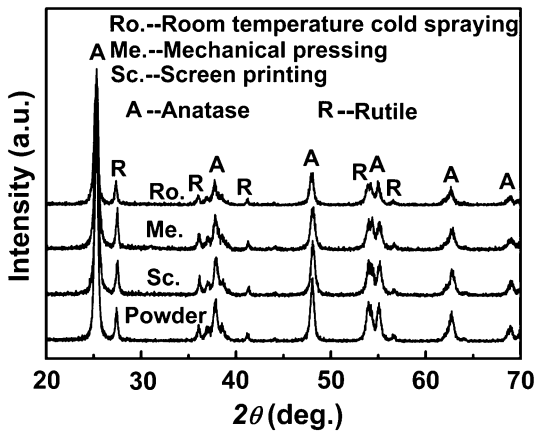

Fig. 1 XRD patterns of the coatings prepared by different processes

ishing both sides down to about 100 μm, and finally dimpling and ion milling (Xe^+) (Gatan 691, Gatan, Oxford, UK) to a thickness thin enough for TEM examination. During TEM experiment, at least five samples for each type of coating were examined.

3. Results and Discussion

3.1 Crystalline Structure of TiO_2 Coatings

Figure 1 shows the XRD patterns of the TiO_2 coatings deposited by different processes in comparison with the starting powder. The TiO_2 starting powder presents mixed crystalline structure of anatase and rutile. It was found that the crystalline structure of TiO_2 coatings does not change after deposition by different processes. This fact indicates that the original crystalline structure of the starting powder can be retained in the coatings prepared by those room temperature processes. As a result, all the coatings have the same crystalline structure as the starting powder.

3.2 Surface Morphologies of TiO_2 Coatings

Figure 2 shows the typical surface morphologies of the TiO_2 coatings deposited by different processes. It can be

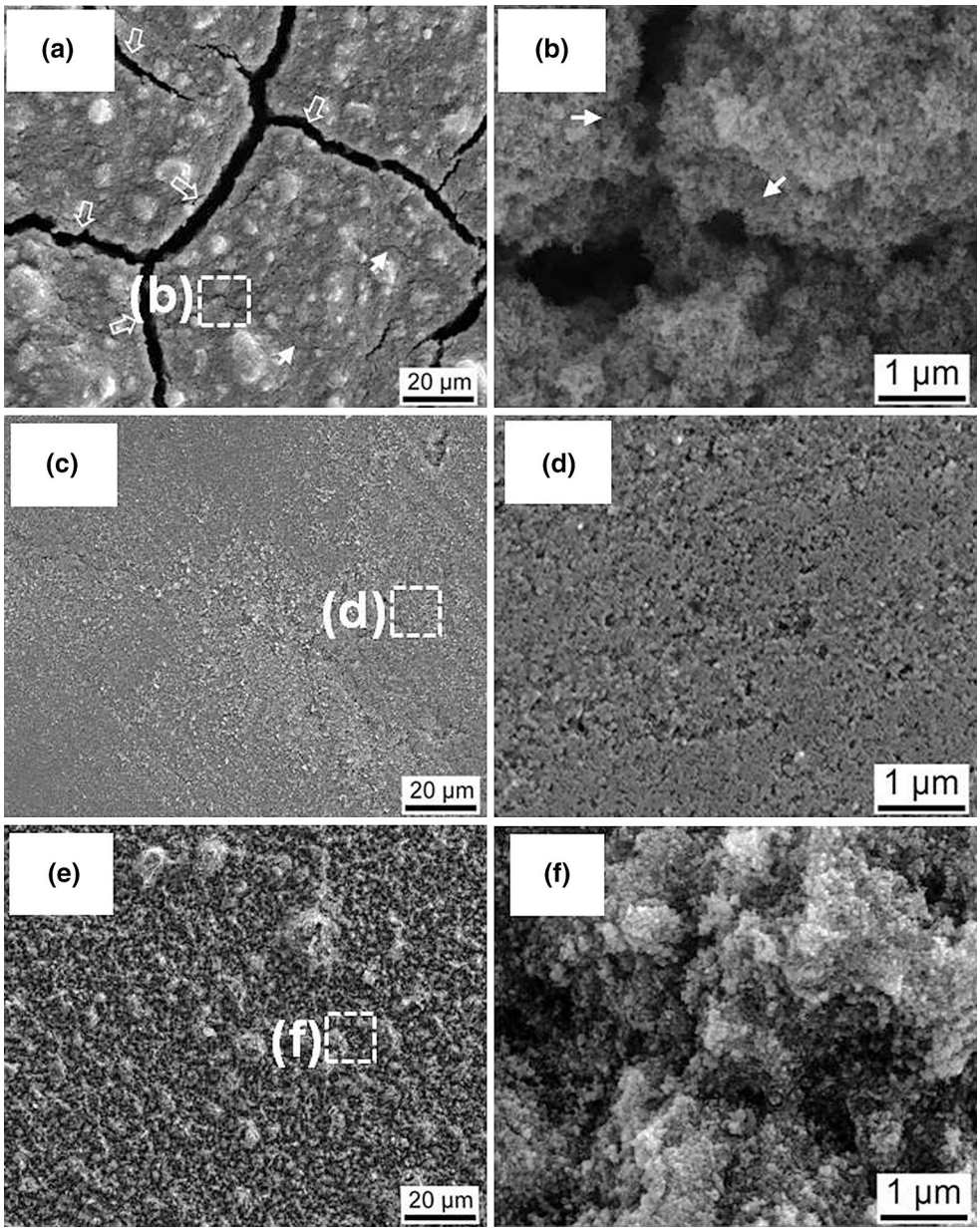

Fig. 2 Surface morphologies of the TiO_2 coatings deposited by different processes. (a) and (b) Non-pressed method of screen printing; (c, d) mechanical pressing; (e, f) room temperature cold spraying. (a, b) Open arrows represent large cracks and solid arrows represent small cracks)

found that the non-pressed TiO_2 coating presented an obvious crack-rich morphology as shown in Fig. 2(a) and (b), including both large cracks (marked by open arrows in Fig. 2a) and small cracks (marked by solid arrows in Fig. 2b). This is because the fracture of the weak bonding between the nano-particles occurred during the drying of the TiO_2 coating, which was also widely reported in literature (Ref 14, 20, 25). Therefore, the process of mechanically pressing was always employed as a post-deposition treatment with an attempt to increase the TiO_2 particles connection and the coating/substrate interface contact. The morphology of the screen-printed coating was significantly altered after pressing (Ref 14, 20, 25). As a result, the mechanical-pressed coating surface became smooth (Fig. 2c) and the cracks were healed as shown in Fig. 2(d). From Fig. 2(e) and (f), the surface morphology of the room temperature cold sprayed coating was rough and no obvious crack on the surface of the coating was observed. During the room temperature cold spraying, the TiO_2 agglomerates with a diameter of hundreds of nanometers are accelerated and then impact on the conductive FTO substrate surface or the deposited coating surface (Ref 17, 18, 30). Consequently, the coating was formed by stacking of the agglomerates as shown in Fig. 2(f).

3.3 Particle/Substrate Interface Contact Modes by TEM Analysis

Figure 3(a) and (b) shows the cross-section and surface morphology of the conductive FTO substrate, respectively. It can be clearly observed that the surface of FTO substrate is rough in nano-scale due to the growth of angular columnar crystals, resulting from the preparation method of magnetron sputtering (Ref 31). Since limited deformation occurs to the substrate during deposition of nano-TiO_2 agglomerates, the nano-TiO_2 particles can be seated on the rough substrate surface inclining toward different directions. This fact causes uncertainty during TEM examination of interface bonding. Therefore, the effective particle/substrate contact in the coating should be distinguished by establishing possible contact modes before examining difference of the coatings deposited by different processes.

During preparing the sample for TEM, organic infill was infiltrated into the coating to avoid destroying mi-

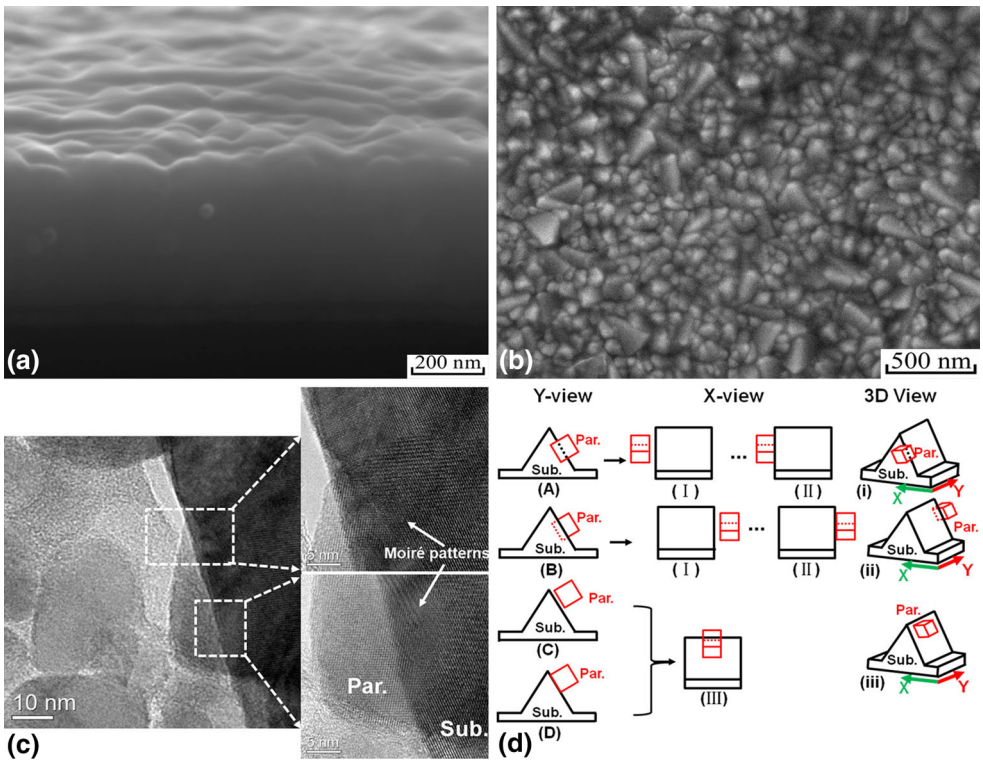

Fig. 3 Schematic modes of particle/substrate contact interface in TEM image. (a) Cross-section image of FTO substrate; (b) surface morphology of FTO substrate; (c) TEM image of overlapped particle/substrate interface in the coating fabricated by screen printing; (d) schematic diagrams of particle/substrate contact modes. ((A-D) Particle/substrate contact mode with the direction along with the electron beam of TEM as shown as Y-view ((A) particle overlapped on substrate, (B) substrate overlapped on particle, (C) separation between particle and substrate, and (D) effective particle/substrate contact); (I-III) particle/substrate contact mode with the direction along with lateral section as shown as X-view ((I) separation between particle and substrate, (II) effective particle/substrate contact and (III) particle overlapped on substrate); (i-iii) schematic 3D view for different contact modes ((i) particle overlapped on substrate, (ii) substrate overlapped on particle, and (iii) separation between particle and substrate or effective particle/substrate contact))

crostructure of the coating/substrate interface during polishing. It was reported that although the sample prepared by focus ions beam (FIB) could be examined by TEM at a low magnification, it is impossible to observe the detail microstructure of the coating/substrate interface of the TiO_2 coating due to the thickness of sample

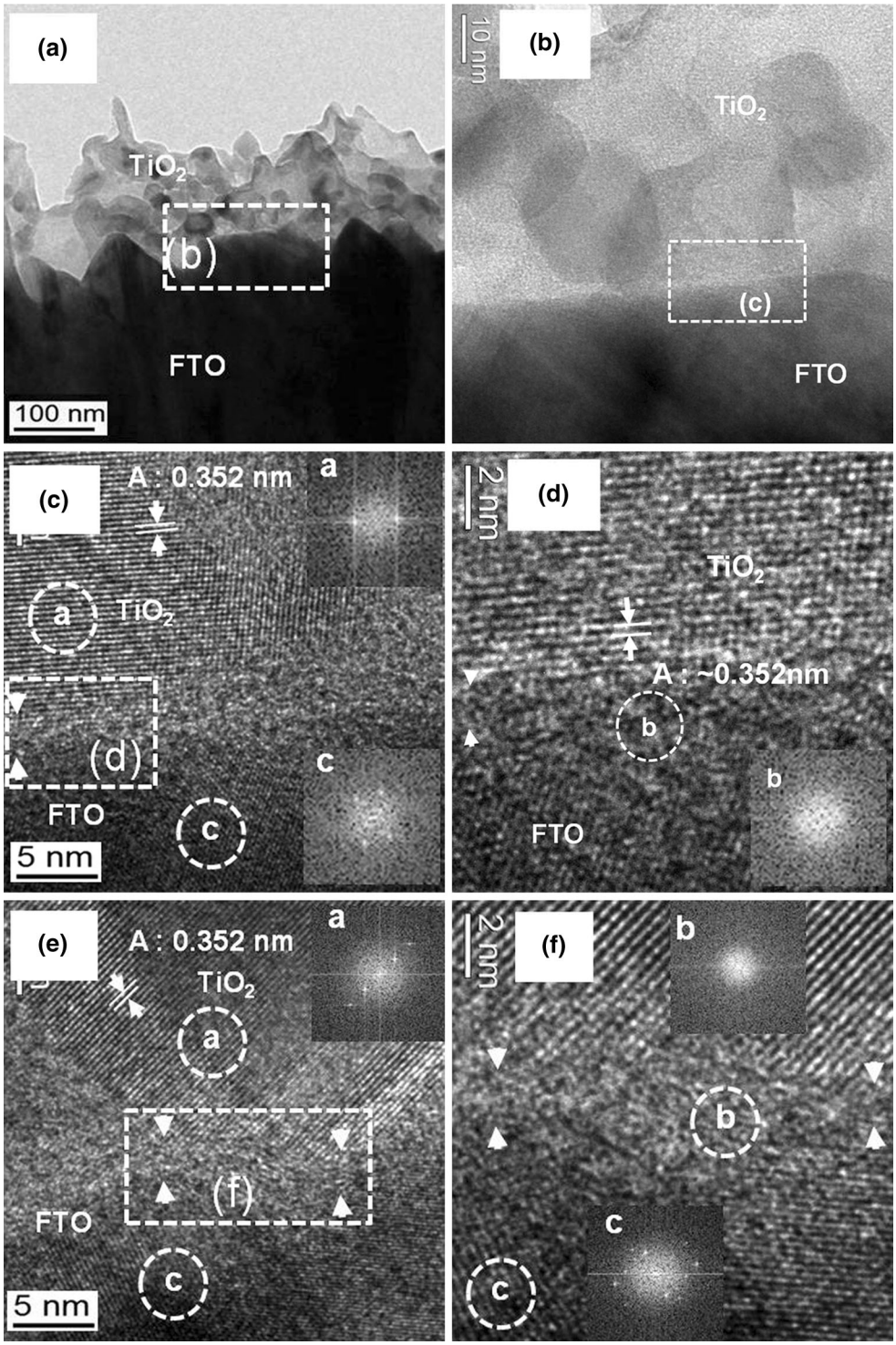

Fig. 4 TEM images of coating/substrate interface for the coating fabricated by screen printing. (a) Low magnification image of the coating/substrate interface; (b-f) High magnification image of the coating/substrate interface for the tabbed zone in (a-c) and (e), respectively. ((c–f) The zones marked as ''a'' represent the TiO_2 particle and its FFT image, the zones marked as ''b'' represent the organics and its FFT image, and the zones marked as ''c'' represent the FTO substrate and its FFT image; white triangle pairs represent the partial contacts)

(ca. 100 nm) (Ref 29). Consequently, the conventional judgment of the coating/substrate contact is just based on whether there is crack at the coating/substrate interface or not (Ref 29). However, the nonbonded interface between coating and substrate does not always exhibit as a crack. Therefore, the judgment of coating/substrate contact based only on crack is not reliable.

By preparing the sample using the method mentioned in section 2.4, the morphological detail for the particle/substrate interface can be observed by high-resolution TEM as shown in Fig. 3(c). In the TEM images, there are different modes for the interface contact between particle and substrate, including separation, overlapping, and effective bonding (as shown in Fig. 3d). For the overlapped particle/substrate interface (case A and case B in Fig. 3d), Moiré patterns (as shown in Fig. 3c) can be observed since the observation direction is along with the electron beam (Ref 32). Due to the observation direction being vertical with the coating/substrate interface (Ref 32), the overlapped contact mode does not mean the effective bonding between particle and substrate being formed. If the observation direction can be along with lateral section of the overlapped particle/substrate interface, it may exhibit different contact modes from separation (Fig. 3d (I)) to effective bonding (Fig. 3d (II)). In fact, it is impossible to characterize the lateral section of the same sample by TEM (Ref 32). Therefore, it is difficult to judge accurately whether the overlapping interface exhibits effective bonding interface due to coexisting two kinds of contact modes (Fig. 3d (I, II)). In contrast, the separation mode for the particle/substrate interface can be easily distinguished in the TEM images (case C in Fig. 3d). Furthermore, the effective bonding mode (case D in Fig. 3d) certainly exhibits an effective particle/substrate contact interface from the viewpoint of the principle of TEM (Ref 32). If the observation direction is along the lateral section of the particle/substrate interface, the separation mode and effective bonding mode may also exhibit an overlapping mode (Fig. 3d (III)). Accordingly, both the separation and overlapping modes in the TEM images cannot be

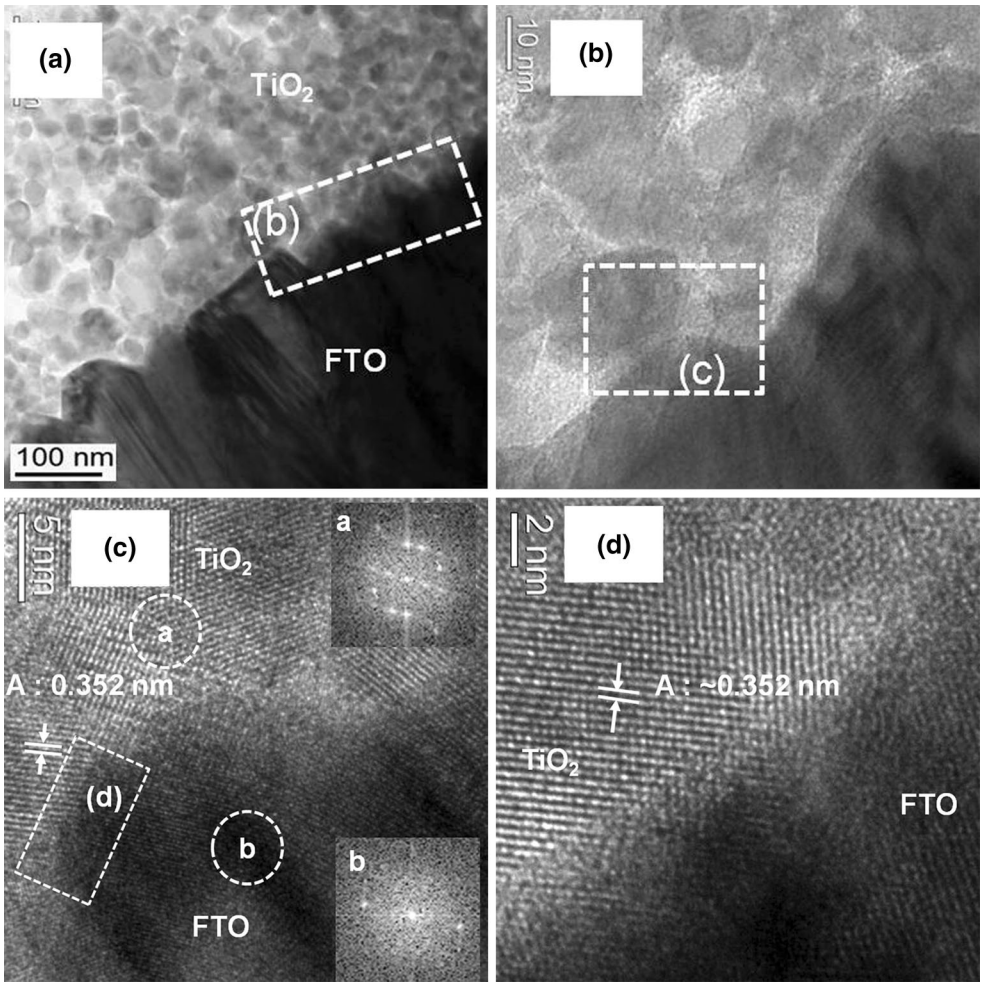

Fig. 5 TEM images of coating/substrate interface for the coating deposited by room temperature cold spraying. (a) Low magnification image of the coating/substrate interface; (b-d) high magnification image of the coating/substrate interface for the tabbed zone in (a-c), respectively. ((c) The zone marked as ''a'' represents the TiO_2 particle and its FFT image, the zone marked as ''b'' represents the FTO substrate and its FFT image)

applied to judge the property of coating/substrate interface contact. The reliable characterization of microstructure for the coating/substrate interface can be realized by only focusing on the effective bonding mode (case D and II in Fig. 3d).

3.4 TEM Morphology of Coating/Substrate Interface for Different Conditions

Figure 4, 5, and 6 show the TEM morphologies of the coating/substrate interface for the coatings prepared by three different processes. In Fig. 4(a), 5(a), and 6(a), the coating/substrate interface can clearly be identified and all the coatings apparently adhered to the substrate surface. However, the differences of the particle/substrate interface contact for the coatings deposited by different processes can be revealed by examining their detailed microstructures.

Figure 4(c-f) shows the typical HRTEM images of the coating/substrate interface for the non-pressed coating. From the inserted FFT images, it can be found that the zones marked as ''a'', ''b,'' and ''c'' represent the TiO_2 particle, the organic infill, and the FTO substrate, respectively. From Fig. 4(c) and (e), no Moiré patterns at the particle/substrate interface can be observed, indicating these particle/substrate contact interfaces belong to the effective bonding mode (case D in Fig. 3d). However, there are only partial contacts between the particles and the substrate (as tabbed by the white triangle pairs in Fig. 4c-f), and these partial contacts were frequently observed at the particle/substrate interface in the non-pressed coating. In addition, the densely stacking of particles on the surface of conductive FTO substrate was hardly observed in the non-pressed coating during TEM examination. This phenomenon is consistent with its high porosity feature (Ref 13, 16). These facts indicate that the particle/substrate interface contact in the non-pressed coating was only formed at limited interface.

Figure 5(b-d) shows the typical HRTEM images of the coating/substrate interface for the room temperature cold sprayed coating. From the inserted FFT images in Fig. 5(c), it can be found that the zones marked as ''a'' and ''b'' represent the TiO_2 particle and the FTO substrate, respectively. In these images, no Moiré patterns were

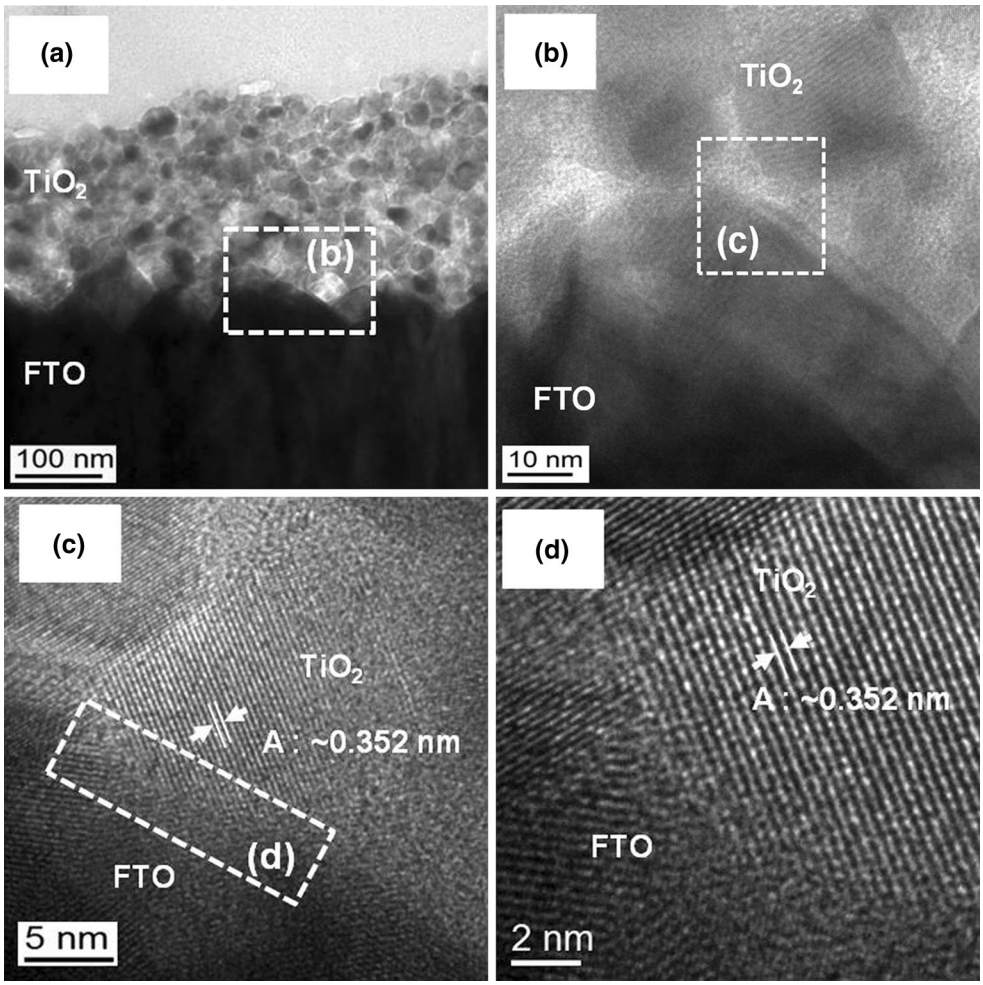

Fig. 6 TEM images of coating/substrate interface for the coating fabricated by mechanical pressing. (a) Low magnification image of the coating/substrate interface; (b-d) high magnification image of the coating/substrate interface for the tabbed zone in (a-c), respectively

observed. This phenomenon indicates that the particle/substrate interface contact belongs to the effective bonding mode (case D in Fig. 3d). Although there existed also partial contacts as shown in the non-pressed coating, the effective bonding was frequently observed at the particle/substrate interface in the room temperature cold sprayed coating. Furthermore, the densely stacking of particles was present nearly at all the substrate surface in the room temperature cold sprayed coating. This result can be attributed to the high impact pressure during room temperature cold spraying, since nano-TiO_2 agglomerates are accelerated to a velocity higher than 100 m/s and then impact on conductive FTO substrate surface (Ref 18). This high velocity impact results in the compaction of deposited particles. Apparently, the near spherical nano-TiO_2 agglomerates deform upon impact to form a hill-like morphology under high impact compressive pressure (Ref 18). Consequently, these effective bonding and densely stacked particles indicate that the particle/substrate interfaces in the room temperature cold sprayed coating are mostly the strongly bonded interfaces.

In Fig. 6, it can be observed that TiO_2 particles effectively adhered to the substrate in the mechanical-pressed coating, and the particles were densely stacked around the surface of conductive FTO substrate. Obviously, the particle/substrate interfaces in the mechanical-pressed coating are similar with that in the room temperature cold sprayed coating. This fact indicates that the strongly bonded particle/substrate interfaces were formed for substantial particles in the pressed coating. Therefore, the particle/substrate interface contact in the pressed coating is superior to that in the non-pressed coating as revealed by HRTEM images. These facts are consistent with higher performance observed for the mechanical-pressed (Ref 14, 20) and room temperature cold sprayed photoanodes (Ref 18) than the non-pressed photoanode.

4. Conclusion

The microstructure details showing the coating/substrate interface contact in the nano-TiO_2 coatings was demonstrated by the HRTEM using ion milling the samples prepared from room temperature cold sprayed, mechanical-pressed, and non-pressed coatings. Surface morphology examination showed that the non-pressed coating is crack-rich, which corresponded to the weak bonding between the nano-particles. The mechanical-pressed and room temperature cold sprayed coatings exhibited continuous morphology without obvious cracks. Although several kinds of contact modes for the particle/substrate interface have been found in the TEM images, only the effective bonding mode could be applied to accurately examine the property of the particle/substrate interface contact. Results showed there were large areas of effective particle/substrate bonding for the room temperature cold sprayed coating and the mechanical-pressed coating. However, only limited interfaces with effective particle/substrate bonding were observed in the non-pressed coating. Those results confirm that both high impact pressure during the room temperature cold spraying and mechanical pressure contributed to the bonding formation at the particle/substrate interface.

Acknowledgments

The work was supported by the National Natural Science Foundation of China (No. 51072160) and the National Program for Support of Top-notch Young Professionals.

References

1. B. O'Regan and M. Gratzel, A Low-Cost, High-Efficiency Solar Cell Based on Dye-Sensitized Colloidal TiO_2 Films, *Nature*, 1991, **353**(6346), p 737-740
2. J.Y. Wang, T.J. Zhang, D.F. Wang, R.K. Pan, Q.Q. Wang, and H.M. Xia, Improved Morphology and Photovoltaic Performance in TiO_2 Nanorod Arrays Based Dye Sensitized Solar Cells by Using a Seed Layer, *J. Alloys Compd.*, 2013, **551**, p 82-87
3. C.J. Raj, S.N. Karthick, A.D. Savariraj, K.V. Hemalatha, P. Song-Ki, H.J. Kim, and K. Prabakar, Electrochemical Properties of TiO_2 Encapsulated ZnO Nanorod Aggregates Dye Sensitized Solar Cells, *J. Alloys Compd.*, 2012, **537**, p 159-164
4. K.M. Lee, V. Suryanarayanan, J.H. Huang, K.R.J. Thomas, J.T. Lin, and K.C. Ho, Enhancing the Performance of Dye-Sensitized Solar Cells Based on an Organic Dye by Incorporating TiO_2 Nanotube in a TiO_2 Nanoparticle Film, *Electrochim. Acta*, 2009, **54**(16), p 4123-4130
5. S.Y. Dai, W.Q. Liu, D.X. Kou, and L.H. Hu, The Kinetics of Electron Transfer Across the Multi-point Contact Interface Through Simplifying the Complex Structure in Dye-Sensitized Solar Cell, *Chem. Phys. Lett.*, 2011, **513**(1-3), p 145-148
6. J. Ferber and J. Luther, Modeling of Photovoltage and Photocurrent in dye-Sensitized Titanium Dioxide Solar Cells, *J. Phys. Chem. B*, 2001, **105**(21), p 4895-4903
7. S. Ruhle and T. Dittrich, Investigation of the Electric Field in TiO_2/FTO Junctions Used in Dye-Sensitized Solar Cells by Photocurrent Transients, *J. Phys. Chem. B*, 2005, **109**(19), p 9522-9526
8. S. Ruhle and D. Cahen, Electron Tunneling at the TiO_2/Substrate Interface Can Determine Dye-Sensitized Solar Cell Performance, *J. Phys. Chem. B*, 2004, **108**(46), p 17946-17951
9. D. Zhao, T.Y. Peng, L.L. Lu, P. Cai, P. Jiang, and Z.Q. Bian, Effect of Annealing Temperature on the Photoelectrochemical Properties of Dye-Sensitized Solar Cells Made with Mesoporous TiO_2 Nanoparticles, *J. Phys. Chem. C*, 2008, **112**(22), p 8486-8494
10. C.P. Hsu, K.M. Lee, J.T.W. Huang, C.Y. Lin, C.H. Lee, L.P. Wang, S.Y. Tsai, and K.C. Ho, EIS Analysis on Low Temperature Fabrication of TiO_2 Porous Films for Dye-Sensitized Solar Cells, *Electrochim. Acta*, 2008, **53**(25), p 7514-7522
11. S. Mori, K. Sunahara, Y. Fukai, T. Kanzaki, Y. Wada, and S. Yanagida, Electron Transport and Recombination in Dye-Sensitized TiO_2 Solar Cells Fabricated Without Sintering Process, *J. Phys. Chem. C*, 2008, **112**(51), p 20505-20509
12. G. Boschloo, J. Lindstrom, E. Magnusson, A. Holmberg, and A. Hagfeldt, Optimization of Dye-Sensitized Solar Cells Prepared by Compression Method, *J. Photochem. Photobiol. A*, 2002, **148**(1-3), p 11-15
13. A. Hagfeldt, G. Boschloo, H. Lindstrom, E. Figgemeier, A. Holmberg, V. Aranyos, E. Magnusson, and L. Malmqvist, A System Approach to Molecular Solar Cells, *Coordin. Chem. Rev.*, 2004, **248**(13-14), p 1501-1509
14. X.C. Zhao, H. Lin, X. Li, and J.B. Li, The Effect of Compression on Electron Transport and Recombination in Plastic TiO_2 Photoanodes, *Electrochim. Acta*, 2011, **56**(18), p 6401-6405

15. T. Yamaguchi, N. Tobe, D. Matsumoto, and H. Arakawa, Highly Efficient Plastic Substrate Dye-Sensitized Solar Cells Using a Compression Method for Preparation of TiO_2 Photoelectrodes, *Chem. Commun.*, 2007, **45**, p 4767-4769
16. H. Lindstrom, A. Holmberg, E. Magnusson, L. Malmqvist, and A. Hagfeldt, A New Method to Make Dye-Sensitized Nanocrystalline Solar Cells at Room Temperature, *J. Photochem. Photobiol. A*, 2001, **145**(1-2), p 107-112
17. S.Q. Fan, G.J. Yang, C.J. Li, G.J. Liu, C.X. Li, and L.Z. Zhang, Characterization of Microstructure of Nano-TiO_2 Coating Deposited by Vacuum Cold Spraying, *J. Therm. Spray Technol.*, 2006, **15**(4), p 513-517
18. G.J. Yang, C.J. Li, K.X. Liao, X.L. He, S. Li, and S.Q. Fan, Influence of Gas Flow During Room Temperature Cold Spraying of Nano-porous TiO_2 Film by Using Strengthened Nanostructured Powder on Performance of Dye-Sensitized Solar Cell, *Thin Solid Films*, 2011, **519**(15), p 4709-4713
19. H.L. Yao, G.J. Yang, S. Li, X.L. He, S.Q. Fan, C.X. Li, and C.J. Li, Synergistic Effects of High Temperature and Impact Compaction on the Nano-TiO_2 Film for the Significant Improvement of Photovoltaic Performance of Flexible Dye-Sensitized Solar Cells, *Electrochim. Acta*, 2013, **87**, p 940-947
20. H.W. Chen, C.Y. Hsu, J.G. Chen, K.M. Lee, C.C. Wang, K.C. Huang, and K.C. Ho, Plastic Dye-Sensitized Photo-supercapacitor Using Electrophoretic Deposition and Compression Methods, *J. Power Sources*, 2010, **195**(18), p 6225-6231
21. M. Durr, A. Schmid, M. Obermaier, S. Rosselli, A. Yasuda, and G. Nelles, Low-Temperature Fabrication of Dye-Sensitized Solar Cells by Transfer of Composite Porous Layers, *Nat. Mater.*, 2005, **4**(8), p 607-611
22. L. Yang, L.Q. Wu, M.X. Wu, G. Xin, H. Lin, and T.L. Ma, High-Efficiency Flexible Dye-Sensitized Solar Cells Fabricated by a Novel Friction-Transfer Technique, *Electrochem. Commun.*, 2010, **12**(7), p 1000-1003
23. M. Manca, F. Malara, L. Martiradonna, L. De Marco, R. Giannuzzi, R. Cingolani, and G. Gigli, Charge Recombination Reduction in Dye-Sensitized Solar Cells by Means of an Electron Beam-Deposited TiO_2 Buffer Layer Between Conductive Glass and Photoelectrode, *Thin Solid Films*, 2010, **518**(23), p 7147-7151
24. J.R. Jennings, Y.R. Liu, F. Safari-Alamuti, and Q. Wang, Dependence of Dye-Sensitized Solar Cell Impedance on Photoelectrode Thickness, *J. Phys. Chem. C*, 2012, **116**(1), p 1556-1562
25. H.C. Weerasinghe, P.M. Sirimanne, G.P. Simon, and Y.B. Cheng, Fabrication of Efficient Solar Cells on Plastic Substrates Using Binder-Free Ball Milled Titania Slurries, *J. Photochem. Photobiol. A*, 2009, **206**(1), p 64-70
26. H.C. Weerasinghe, G.V. Franks, J.D. Plessis, G.P. Simona, and Y.B. Cheng, Anomalous Rheological Behavior In Chemically Modified TiO_2 Colloidal Pastes Prepared for Flexible Dye-Sensitized Solar Cells, *J. Mater. Chem. A*, 2010, **20**, p 9954-9961
27. G.J. Yang, C.J. Li, S.Q. Fan, Y.Y. Wang, and C.X. Li, Influence of Annealing on Photocatalytic Performance and Adhesion of Room Temperature Cold-Sprayed Nanostructured TiO_2 Coating, *J. Therm. Spray Technol.*, 2007, **16**(5-6), p 873-880
28. X.L. He, G.J. Yang, C.J. Li, and C.X. Li, Influence of Accelerating Gas Flow Rate on the Particle Cohesion in Room-Temperature Cold-Sprayed Scattering Layer for Plastic-Based Dye-Sensitized Solar Cells, *Appl. Surf. Sci.*, 2014, **288**, p 416-422
29. P. de Almeida, J. van Deelen, C. Catry, H. Sneyers, T. Pataki, R. Andriessen, C. Van Roost, and J.M. Kroon, Microstructure Characterization of Titanium Dioxide Nanodispersions and Thin Films for Dye-Sensitized Solar Cell Devices, *Appl. Phys. a-Mater.*, 2004, **79**(7), p 1819-1828
30. G.J. Yang, C.J. Li, S.Q. Fan, and J.C. Gao, Influence of Pore Structure on Ion Diffusion Property in Porous TiO_2 Coating and Photovoltaic Performance of Dye-Sensitized Solar Cells, *Surf. Coat. Technol.*, 2011, **205**(10), p 3205-3210
31. B.H. Liao, S.H. Chan, C.C. Lee, C.C. Kuo, S.H. Chen, and D. Chiang, FTO Films Deposited in Transition and Oxide Modes by Magnetron Sputtering Using Tin Metal Target, *Appl. Opt.*, 2014, **53**(4), p 148-153
32. Z.L. Wang, *Characterization of Nanophase Materials*, Wiley-VCH Verlag GmbH, Weinheim, 2000, p 37-80